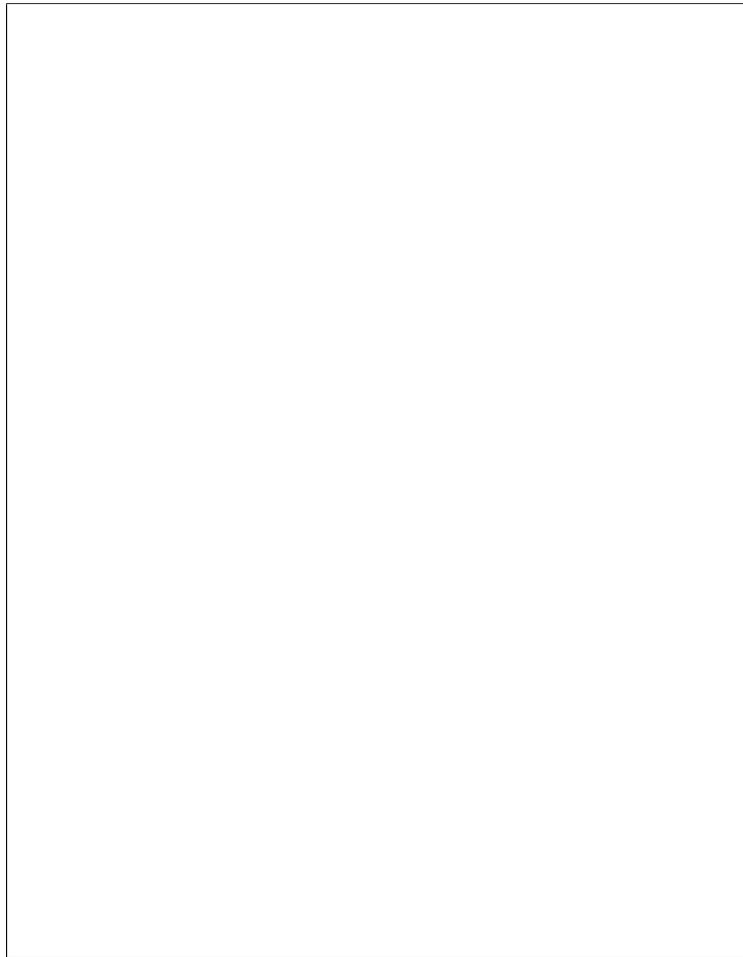


**Provided for non-commercial research and education use.
Not for reproduction, distribution or commercial use.**



This article appeared in a journal published by Elsevier. The attached copy is furnished to the author for internal non-commercial research and education use, including for instruction at the authors institution and sharing with colleagues.

Other uses, including reproduction and distribution, or selling or licensing copies, or posting to personal, institutional or third party websites are prohibited.

In most cases authors are permitted to post their version of the article (e.g. in Word or Tex form) to their personal website or institutional repository. Authors requiring further information regarding Elsevier's archiving and manuscript policies are encouraged to visit:

<http://www.elsevier.com/authorsrights>

Contents lists available at [ScienceDirect](#)

Geomechanics for Energy and the Environment

journal homepage: www.elsevier.com/locate/gete

Ground heave due to line injection sources

Jueun Kim¹, A.P.S. Selvadurai^{*,2}

Department of Civil Engineering and Applied Mechanics, McGill University, 817 Sherbrooke Street West, Montreal, QC, Canada, H3A 0C3

HIGHLIGHTS

- An analytical solution for the poroelastic problem associated with a line injection sources is developed.
- Numerical results that can be used as a first approximation of ground heave for different line injection lengths are presented.
- The potential of failure development at the injection zone is examined.
- Provides validation of a computational approach.

ARTICLE INFO

Article history:

Received 26 November 2014

Received in revised form 17 February 2015

Accepted 7 March 2015

Available online 18 March 2015

Keywords:

Biot poroelasticity

Pressurized reservoirs

Geologic sequestration

Tensile stress states

Failure potential

ABSTRACT

This paper examines the geomechanical effects resulting from the injection of a non-reactive fluid along a line segment located at the interior of a poroelastic halfspace. The mechanical behaviour of the geologic medium is described using Biot's classical theory of poroelasticity. The mathematical solutions for the surface heave associated with a point injection source are used to develop results for the ground heave associated with both vertically-aligned and horizontally-aligned line injection sources of constant intensity and finite length. The results obtained from the mathematical analysis are used to benchmark computational results for analogous problems.

© 2015 Elsevier Ltd. All rights reserved.

1. Introduction

The behaviour of fluid-saturated geological media due to injection of fluids at the interior has important applications to the geologic sequestration of fluidized greenhouse gases (Rutqvist,¹ Selvadurai^{2,3}) and geologic disposal of contaminants and hazardous wastes in fluidized forms.^{4–12} Pressurized injection of fluids to the interior of a geologic medium can alter the stress state in the porous skeleton and in the pore fluids. It is therefore important to assess the influences of injection activities so that the geomechanical implications, particularly in terms of potential for fracture

generation and failure in the geologic medium, can be adequately assessed. The failure of geologic media during injection is an important consideration in energy resources extraction endeavours (e.g. shale gas extraction). The injection of fluids to the interior of geological media can result in ground heave. This aspect is also important to engineering implementation of geologic sequestration of fluidized greenhouse gas. Recent CO₂ injection activities in In Salah, Algeria have resulted in time-dependent heave of the ground surface (Fig. 1) (see e.g. Vasco et al.¹³). Ground heave can result in additional stress that can lead to failure of geological media. The majority of studies in this area treat the injection activity as a static process where the geologic medium is assumed to be an elastic solid and the *injection* process is simulated by a distribution of centres of dilatation acting at the interior of the geologic formation. Examples of such studies are given by Geertsma,¹⁴ Segall,¹⁵ Segall and Fitzgerald¹⁶ and more recently by Selvadurai.^{2,3} Within the scope of the theory of linear poroelasticity, the

* Corresponding author.

E-mail address: patrick.selvadurai@mcgill.ca (A.P.S. Selvadurai).

¹ Graduate Student.

² William Scott Professor and James McGill Professor.

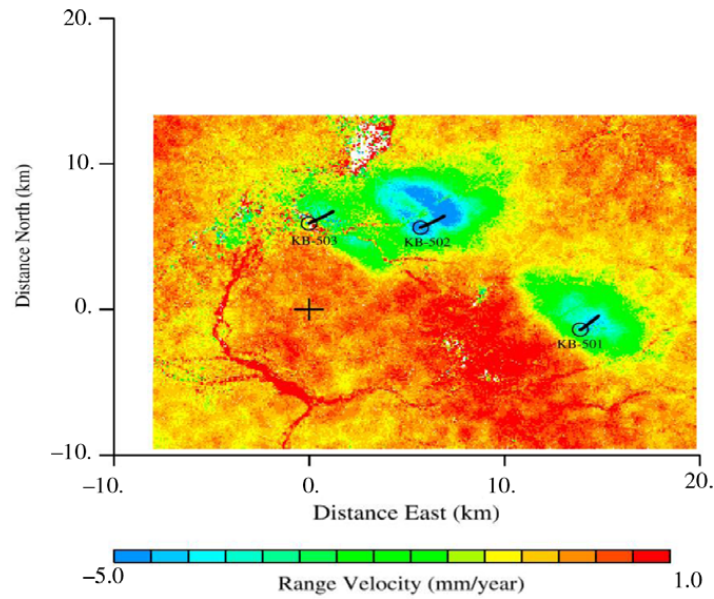


Fig. 1. Example of the ground heave due to CO₂ injection (Fig. 1 given in Vasco et al.¹³).

solutions at $t = 0$ and $t \rightarrow \infty$ are essentially elasticity solutions. The fluid injection process is, however, a transient problem and the stress state in the geological medium can be influenced by the rate of injection. Therefore it is important to pose the fluid injection problem within the context of the theory of poroelasticity so that the influence of the injection rate, the fluid transport properties, etc., can be incorporated in the study of the injection problem. An objective of this paper is to extend the existing modelling to include transient poromechanical behaviour of the geologic medium and to simulate the injection process so that the time-dependent ground heave and the stress state at critical locations of the geological formation can be assessed in terms of non-dimensional parameter groups associated with the poroelastic properties and the injection processes.

The classical theory of poromechanics, as developed by Biot,¹⁷ provides a suitable phenomenological model for examining the coupled processes encountered in fluid-saturated porous media. The basic theory takes into consideration the transient effects associated with the coupling of fluid flow and elastic deformations in a fluid-saturated porous medium. Extensive accounts of developments in this area and alternative representations of Biot's governing equations are given by Rice and Cleary,¹⁸ Detournay and Cheng,¹⁹ Coussy,²⁰ Selvadurai,^{21,22} Selvadurai and Yue,²³ Yue et al.,²⁴ Selvadurai and Shirazi²⁵ and Verruijt.²⁶ Despite simplifications associated with the assumption of linear elastic behaviour of the porous skeleton and Darcy flow through the porous skeleton, the theory continues to be the mainstay of approaches associated with the solution of many important problems in geosciences and geomechanics relevant to groundwater extraction and recharge,^{27,14,28–30} geologic disposal of heat-emitting nuclear waste,^{4,5,11,12} geologic sequestration of greenhouse gases in fluidized forms^{31,32} and deep mantle processes and seismic effects.^{33,34}

This paper examines the geomechanical response of the fully saturated porous medium resulting from fluid injection into the interior region. The mathematical solution

for the axisymmetric point source problem is used to develop results for line source injection problems. Integral transform techniques (Hankel and Laplace transform techniques) are used in the solution of the point source injection problem. The results are converted to 3-dimensional solutions by taking double Fourier transforms instead of Hankel transforms. It is shown that the mathematical solutions for horizontally and vertically aligned line sources can be obtained by superposing the point source solutions. The analytical results are also used to assess the accuracy of the computational results obtained from the finite element-based multi-physics code, COMSOLTM.

2. Governing equations

The constitutive equations for linear, isotropic and isothermal poroelasticity were first given by Biot¹⁷ and rederived and extended in terms of engineering parameters by Rice and Cleary¹⁸ (see also Detournay and Cheng¹⁹; Selvadurai and Yue²³; Yue and Selvadurai³⁵; Selvadurai^{21,22}):

$$\boldsymbol{\sigma} = 2G\boldsymbol{\epsilon} + \frac{2G\nu}{1-2\nu}\text{tr}\boldsymbol{\epsilon}\mathbf{I} - \frac{3(\nu_u - \nu)}{B(1-2\nu)(1+\nu_u)}p\mathbf{I} \quad (1)$$

$$p = \frac{2GB^2(1-2\nu)(1+\nu_u)^2}{9(\nu_u - \nu)(1-2\nu_u)}\Theta - \frac{2GB(1+\nu_u)}{3(1-2\nu_u)}\text{tr}\boldsymbol{\epsilon} \quad (2)$$

where p is the pore pressure, $\boldsymbol{\epsilon}$ is the strain tensor, $\boldsymbol{\sigma}$ is the total stress, Θ is the volumetric strain, G is the shear modulus, ν is the Poisson's ratio, ν_u is the undrained Poisson's ratio, and B is the Skempton's pore pressure parameter.³⁶ Darcy's law governing flow of the fluid through the porous medium is given by

$$\mathbf{v} = -\frac{k}{\gamma_w}\nabla p \quad (3)$$

where \mathbf{v} is the velocity of the fluid and k is the hydraulic conductivity. In Eq. (3), we assume that the velocity of the porous skeleton is small in comparison to the

velocity of the pore fluid and therefore can be neglected in the formulation of Darcy's law. Substituting Eqs. (1)–(3) into the equations of equilibrium and the mass conservation equation of the pore fluid gives rise to the basic equations governing the theory of poroelasticity in terms of the displacements and the pore fluid pressure. We first restrict attention to a state of axial symmetry in the fluid injection process into an interior point. The axisymmetric form of the basic equations governing Biot's poroelasticity can be written as

$$G \left(\nabla^2 u_r - \frac{u_r}{r^2} \right) - (2\eta - 1) \frac{\partial \Theta}{\partial r} = \alpha \frac{\partial p}{\partial r} \quad (4)$$

$$G \nabla^2 u_z - (2\eta - 1) \frac{\partial \Theta}{\partial z} = \alpha \frac{\partial p}{\partial z} \quad (5)$$

$$\beta \frac{\partial p}{\partial t} - \gamma \frac{\partial \Theta}{\partial t} = c \nabla^2 p \quad (6)$$

where

$$\begin{aligned} \alpha &= \frac{3(\nu_u - \nu)}{B(1 - 2\nu)(1 + \nu_u)}; \\ \beta &= \frac{(1 - 2\nu_u)(1 - \nu)}{(1 - 2\nu)(1 - \nu_u)}; \\ \gamma &= \frac{2GB(1 - \nu)(1 + \nu_u)}{3(1 - 2\nu)(1 - \nu_u)} \\ c &= \frac{2GB^2(1 - \nu)(1 + \nu_u)^2 k}{9(\nu_u - \nu)(1 - \nu_u)\gamma_w}; \quad \eta = \frac{(1 - \nu)}{(1 - 2\nu)} \end{aligned} \quad (7)$$

and ∇^2 is the axisymmetric form of Laplace's operator given by

$$\nabla^2 = \frac{\partial^2}{\partial r^2} + \frac{1}{r} \frac{\partial}{\partial r} + \frac{\partial^2}{\partial z^2}. \quad (8)$$

To ensure positive definiteness of the strain energy potential, the material parameters should satisfy the following thermodynamic constraints; $G > 0, 0 \leq B \leq 1; -1 < \nu < \nu_u \leq 0.5$. (see e.g. Rice and Cleary¹⁸; Detournay and Cheng¹⁹; Wang³⁷ and further references are given in Selvadurai^{21,22}).

2.1. Methods of solution of the governing equations

We introduce displacement functions $S(r, z, t)$ and $E(r, z, t)$ (see e.g. McNamee and Gibson^{38,39}) where the displacement and stress components can be expressed in the forms

$$\begin{aligned} u_r &= -\frac{\partial E}{\partial r} + z \frac{\partial S}{\partial r}; \quad u_z = -\frac{\partial E}{\partial z} + z \frac{\partial S}{\partial z} - S; \\ \Theta &= \nabla^2 E; \quad p = \frac{2G}{\alpha} \left(\frac{\partial S}{\partial z} - \eta \Theta \right) \end{aligned} \quad (9)$$

$$\begin{aligned} \frac{\sigma_{rr}}{2G} &= \left(\frac{\partial^2}{\partial r^2} - \nabla^2 \right) E - z \frac{\partial^2 S}{\partial r^2} + \frac{\partial S}{\partial z}; \\ \frac{\sigma_{zz}}{2G} &= \left(\frac{\partial^2}{\partial z^2} - \nabla^2 \right) E - z \frac{\partial^2 S}{\partial z^2} + \frac{\partial S}{\partial z}; \\ \frac{\sigma_{rz}}{2G} &= \frac{\partial^2 E}{\partial r \partial z} - z \frac{\partial^2 S}{\partial r \partial z}. \end{aligned} \quad (10)$$

The coupled system of partial differential equations governing $S(r, z, t)$ and $E(r, z, t)$ takes the forms

$$\nabla^2 S = 0 \quad (11)$$

$$c \nabla^4 E = \left(\beta + \frac{\alpha \gamma}{2G\eta} \right) \nabla^2 \frac{\partial E}{\partial t} - \frac{\beta}{\eta} \frac{\partial^2 S}{\partial z \partial t}. \quad (12)$$

We introduce the zeroth-order Hankel transform with respect to the radial coordinate (r) and the Laplace transform with respect to the time (t), such that

$$\bar{F}(\xi, z, t) = \int_0^\infty r J_0(\xi r) F(r, z, t) dr \quad (13)$$

$$\tilde{F}(r, z, s) = \frac{1}{2\pi i} \int_0^\infty e^{-st} F(r, z, t) dt. \quad (14)$$

The PDEs governing Eqs. (11) and (12) give the following system of the coupled ODEs for the transformed variables $\bar{S}(r, z, t)$ and $\tilde{E}(r, z, t)$: i.e.

$$\left(\frac{d^2}{dz^2} - \xi^2 \right) \bar{S} = 0 \quad (15)$$

$$\begin{aligned} \left(\frac{d^2}{dz^2} - \xi^2 \right) \left\{ \frac{d^2}{dz^2} - \left[\xi^2 + \frac{s}{c} \left(\beta + \frac{\alpha \gamma}{2G\eta} \right) \right] \right\} \tilde{E} \\ = -\frac{\beta s}{\eta c} \frac{d\bar{S}}{dz}. \end{aligned} \quad (16)$$

3. Fluid injection at a point in the halfspace

We first examine the problem of injection of a fluid at a constant rate into a point within the poroelastic halfspace. The injection of fluid occurs at a constant volume flow rate of Q_0 (units L^3/T) at a point located at a finite depth h from the traction free surface (Fig. 2). For convenient formulation, we introduce the superscript $()^L$ to indicate the layer occupying the region $r \in (0, \infty); z \in (0, -h)$, and the superscript $()^H$ to indicate the halfspace occupying the region $r \in (0, \infty); z \in (0, \infty)$ (Fig. 2).

The boundary conditions applicable to the surface $z = -h$ are

$$\begin{aligned} \sigma_{zz}^L(r, -h, t) = 0; \quad \sigma_{rz}^L(r, -h, t) = 0; \\ p^L(r, -h, t) = 0. \end{aligned} \quad (17)$$

And, at the interface $z = 0$, the continuity conditions are

$$u_r^L(r, 0, t) - u_r^H(r, 0, t) = 0; \quad u_z^L(r, 0, t) - u_z^H(r, 0, t) = 0 \quad (18)$$

$$\begin{aligned} \sigma_{zz}^L(r, 0, t) - \sigma_{zz}^H(r, 0, t) = 0; \\ \sigma_{rz}^L(r, 0, t) - \sigma_{rz}^H(r, 0, t) = 0 \end{aligned} \quad (19)$$

$$p^L(r, 0, t) - p^H(r, 0, t) = 0. \quad (20)$$

A velocity discontinuity occurs due to the influx of fluid into a point at the interface (see e.g. Kanok-Nukulchai and Chau³⁰)

$$\frac{k}{\gamma_w} \left(\frac{\partial p}{\partial z} \right)_{z=0}^L - \frac{k}{\gamma_w} \left(\frac{\partial p}{\partial z} \right)_{z=0}^H = \frac{Q_0 \delta(r)}{2\pi r} H(t) \quad (21)$$

where $\delta(r)$ is the Dirac delta function (which has units of $1/\text{Length}$) and $H(t)$ is the Heaviside step function. The initial conditions governing the poroelasticity problem are

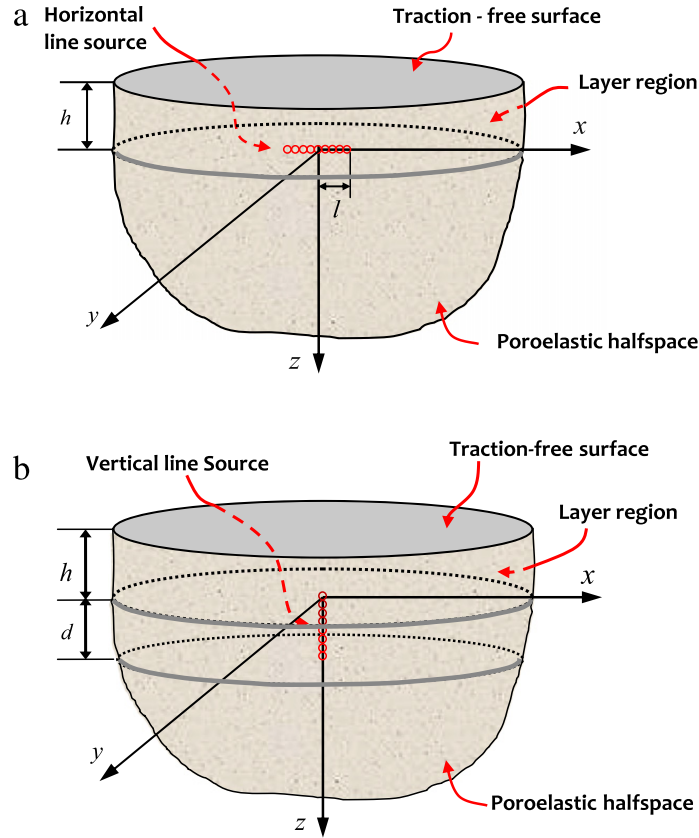


Fig. 2. Line source injection into a poroelastic halfspace formulated by superposing a number of point sources along the line. (a) Horizontal line source injection; (b) Vertical line source injection.

$$\begin{aligned} \sigma^L(\mathbf{x}, 0) = \sigma^H(\mathbf{x}, 0) = \mathbf{u}^L(\mathbf{x}, 0) = \mathbf{u}^H(\mathbf{x}, 0) = 0 \\ p^L(\mathbf{x}, 0) = p^H(\mathbf{x}, 0) = 0. \end{aligned} \quad (22)$$

In addition, the solution should satisfy the regularity condition, which requires

$$\begin{aligned} \sigma^{(i)}(\mathbf{x}, t), \quad p^{(i)}(\mathbf{x}, t), \quad \mathbf{u}^{(i)}(\mathbf{x}, t) \rightarrow 0, \\ (i = L, H) \quad \text{as } |\mathbf{x}| \rightarrow \infty, \quad t \in (0, \infty). \end{aligned} \quad (23)$$

4. Final results for the poroelasticity problem

The solution to the point source injection problem has been obtained by several authors^{28–30,40,41} and the extraction problem for a disc-shaped source of infinitesimal thickness has recently been developed by Selvadurai and Kim.⁴² A result of importance to the analysis of ground heave is the vertical displacement $u_z(r, z, t)$ that occurs on the surface of the halfspace region. Avoiding details of the mathematical manipulation, the final expression for the vertical displacement can be represented in the form

$$\begin{aligned} \frac{u_z^L(r, z, t)}{Q_0 \gamma_w \alpha / 2G(2\pi)k} = & \int_{\zeta-i\infty}^{\zeta+i\infty} \int_0^\infty \xi J_0(r\xi) \\ & \times \left\{ \left(\frac{e^{-\xi h} - e^{-\varphi h}}{\eta \Gamma(\varphi - \xi)^2 - \eta(\varphi^2 - \xi^2) + \xi(\varphi - \xi)} \right) \right. \\ & \times \left[(\xi \Gamma(z+h) - \Gamma - \xi(z+h)) e^{-\xi z - \xi h} \right. \\ & \left. \left. + \frac{(2\eta \xi \Gamma - \xi)}{\eta(\varphi^2 - \xi^2)} (\varphi e^{-\varphi z - \varphi h} - \xi e^{-\xi z - \xi h}) \right] \right. \end{aligned}$$

$$\begin{aligned} & \left. + \xi (e^{-\xi z - \xi h} + e^{\xi z + \xi h}) \frac{e^{-\xi h}}{2\eta \xi (\varphi^2 - \xi^2)} \right. \\ & \left. + \varphi (e^{-\varphi z - \varphi h} + e^{\varphi z + \varphi h}) \frac{-e^{-\varphi h}}{2\eta \varphi (\varphi^2 - \xi^2)} \right\} \frac{e^{st}}{s} d\xi ds \quad (24) \end{aligned}$$

where ζ is a real number-associated Bromwich integral used in the Laplace transform inversion and

$$\varphi = \sqrt{\xi^2 + \frac{s}{c} \left(\beta + \frac{\alpha \gamma}{2G\eta} \right)}; \quad \Gamma = \frac{\beta G}{2\eta \beta G + \alpha \gamma}. \quad (25)$$

Using the relationship between the Hankel transforms and Fourier transforms,^{43,44} this mathematical form is converted into a three-dimensional solution by introducing a double Fourier transform with respect to x and y instead of taking the Hankel transform with respect to r . The double Fourier transform is defined by

$$\hat{F}(u, v, z, t) = \int_{-\infty}^{\infty} \int_{-\infty}^{\infty} F(x, y, z, t) e^{-i(ux+vy)} dx dy. \quad (26)$$

The solution for the vertical displacement expressed in rectangular Cartesian coordinates can then be written as Eq. (27) given in Box I. Expressions for the double Fourier equivalents of the axial displacement $u_z(\mathbf{x}, t)$, pore fluid pressure $p(\mathbf{x}, t)$ and total stresses $\sigma_{ij}(\mathbf{x}, t)$ are also obtained using a similar procedure. Relevant results for the stresses and displacements are given in the Appendix (Boxes IV to X).

$$\begin{aligned}
 \frac{u_z^L(x, y, z, t)}{Q_0 \gamma_w \alpha / 2G(2\pi)^2 k} &= \int_{\zeta-i\infty}^{\zeta+i\infty} \int_{-\infty}^{\infty} \int_{-\infty}^{\infty} e^{i(ux+vy)} \\
 &\times \left\{ \left(\frac{e^{-\sqrt{u^2+v^2}h} - e^{-\varphi h}}{\eta \Gamma(\varphi - \sqrt{u^2+v^2})^2 - \eta(\varphi^2 - \sqrt{u^2+v^2}) + \sqrt{u^2+v^2}(\varphi - \sqrt{u^2+v^2})} \right) \right. \\
 &\times \left[(\sqrt{u^2+v^2}(z+h)(\Gamma-1) - \Gamma)e^{-\sqrt{u^2+v^2}(z+h)} + \frac{(2\eta\sqrt{u^2+v^2}\Gamma - \sqrt{u^2+v^2})}{\eta(\varphi^2 - \sqrt{u^2+v^2})} (\varphi e^{-\varphi(z+h)} \right. \\
 &- \sqrt{u^2+v^2}e^{-\sqrt{u^2+v^2}(z+h)}) + \sqrt{u^2+v^2}(e^{-\sqrt{u^2+v^2}(z+h)} + e^{\sqrt{u^2+v^2}(z+h)}) \frac{e^{-\sqrt{u^2+v^2}h}}{2\eta\sqrt{u^2+v^2}(\varphi^2 - \sqrt{u^2+v^2})} \\
 &\left. \left. + \varphi(e^{-\varphi(z+h)} + e^{\varphi(z+h)}) \frac{-e^{-\varphi h}}{2\eta\varphi(\varphi^2 - \sqrt{u^2+v^2})} \right) \right\} \times \frac{e^{st}}{s} dudvds \quad (27)
 \end{aligned}$$

Box I.

[Note that the designations $\sqrt{u^2+v^2}$ and $\sqrt{u^2+v^2}$ in (27) (and subsequent expressions) are used to emphasize the fact that the solutions are obtained through the application of a Fourier transform rather than a Hankel transform. The Hankel transform variable ξ is $\sqrt{u^2+v^2}$ in the Fourier domain and ξ^2 is $\sqrt{u^2+v^2}$ in the Fourier domain.]

4.1. Distributed injection problems 1: Horizontal line source

We consider the problem of fluid injection along a horizontal line situated at a depth h from the surface of the poroelastic halfspace (Fig. 2(a)). The problem can be formulated in a variety of ways including the superposition technique. Assuming that the line source consists of a number of point sources placed along the line, the solution for the horizontal line injection problem can be obtained by superposing the point source solutions either discretely or continuously. Using the integral technique, the surface displacement for the horizontal line injection problem can be obtained from the result

$$\begin{aligned}
 u_z^L(x, y, -h, t)_{(\text{Horizontal line source})} \\
 = \int_{-l}^l U_z^L(x, y, -h, \xi^*, t)_{(\text{Point source})} d\xi^* \quad (28)
 \end{aligned}$$

where $U_z^L(x, y, -h, \xi^*, t)_{(\text{Point source})}$ is given by Eq. (29) given in Box II.

The complete solution for the horizontal line source is obtained by utilizing this superposition technique.

4.2. Distributed injection problems 2: Vertical line source

The solution to the problem of the axial surface displacement due to fluid injection along a line source located on the z -axis can be obtained in the form

$$\begin{aligned}
 u_z^L(x, y, -h, t)_{(\text{Vertical line source})} \\
 = \int_0^d U_z^L(x, y, -h, \eta^*, t)_{(\text{Point source})} d\eta^* \quad (30)
 \end{aligned}$$

where $U_z^L(x, y, -h, \eta^*, t)_{(\text{Point source})}$ is given by Eq. (31) given in Box III.

5. Analytical solutions and comparison with computations

Formal analytical solutions for the vertical displacements and pore fluid pressure for the cases involving injection along a horizontally- or a vertically-oriented line source of finite length have been developed. The final analysis of the problem is completed with the inversion of both the Fourier and Laplace transforms. An exact inversion of these transforms is not possible but numerical inversion procedures available in MATLAB[®] can be used. The Laplace transform inversion is performed using the algorithm developed by Crump.⁴⁵ The validation of these numerical schemes for the axisymmetric case is further discussed in Selvadurai and Kim.⁴²

The computational solutions were obtained using the finite element-based multi-physics code COMSOL[™]. The horizontal and vertical line source problems are 3-dimensional problems, and the representation of the COMSOL[™] modelling is shown in Fig. 3. The influence of a finite boundary is minimized by locating the exterior boundary of the domain at a distance sufficiently remote from the fluid injection location (i.e. the dimensions of the discretized domain are $x \in (-100l, 100l)$; $y \in (-100l, 100l)$; $z \in (0, 100h)$). At the surface, the pore pressure and the effective stress are set to zero, and a flux discontinuity is applied to the interface between the layer and the halfspace. The symmetry/zero flux boundary condition is applied at the bottom and the lateral surfaces. Fig. 4 shows the mesh configuration used in the COMSOL[™] modelling. Extra fine meshes are used around the injection region, and coarse meshes are used for the rest of the domain. The mesh consists of 11,616 tetrahedral elements for $l/h = 0.1$ and increases to 23,817 for $l/h = 10$. Each nodal point has 4 degrees of freedom (DOF).

In the computational modelling, the following values were used to evaluate the surface displacements, the pore fluid pressure and the effective stresses (the geological medium has properties similar to limestone given in Hart and Wang⁴⁶ and Selvadurai and Najari⁴⁷):

$$\begin{aligned}
 G &= 20.0 \times 10^3 \text{ kN/m}^2; & \nu &= 0.25; & k &= 10^{-5} \text{ m/s}; \\
 \gamma_w &= 9.81 \text{ kN/m}^3; & \nu_u &= 0.5.
 \end{aligned}$$

$$\frac{U_z^L(x, y, -h, \xi^*, t)}{Q_0 \gamma_w \alpha / 2G(2\pi)^2 k} = \int_{\zeta=-i\infty}^{\zeta+i\infty} \int_{-\infty}^{\infty} \int_{-\infty}^{\infty} e^{i(u(x-\xi^*)+vy)} \times \left(\frac{e^{-\sqrt{u^2+v^2}h} - e^{-\varphi h}}{\eta \Gamma(\varphi - \sqrt{u^2+v^2})^2 - \eta(\varphi^2 - \sqrt{u^2+v^2}) + \sqrt{u^2+v^2}(\varphi - \sqrt{u^2+v^2})} \right) \times \frac{e^{st}}{s} dudvds \quad (29)$$

Box II.

$$\frac{U_z^L(x, y, -h, \eta^*, t)}{Q_0 \gamma_w \alpha / 2G(2\pi)^2 k} = \int_{\zeta=-i\infty}^{\zeta+i\infty} \int_{-\infty}^{\infty} \int_{-\infty}^{\infty} e^{i(ux+vy)} \times \left(\frac{e^{-\sqrt{u^2+v^2}(h+\eta^*)} - e^{-\varphi(h+\eta^*)}}{\eta \Gamma(\varphi - \sqrt{u^2+v^2})^2 - \eta(\varphi^2 - \sqrt{u^2+v^2}) + \sqrt{u^2+v^2}(\varphi - \sqrt{u^2+v^2})} \right) \times \frac{e^{st}}{s} dudvds. \quad (31)$$

Box III.

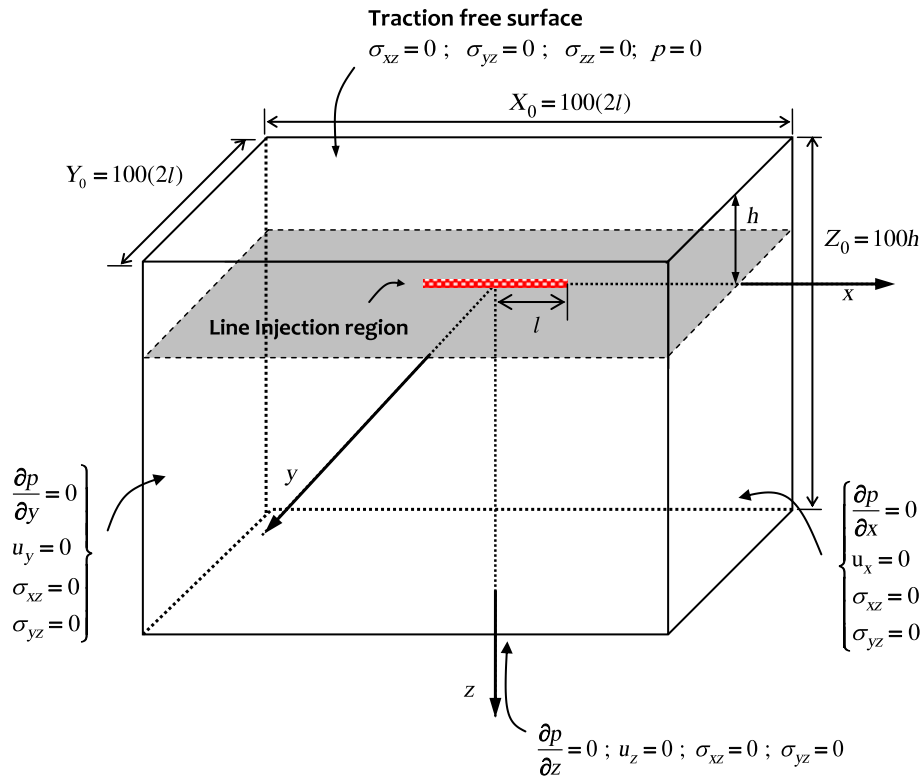


Fig. 3. The geometry of the region used in COMSOL™ modelling.

5.1. Point source

Fig. 5 compares the analytical solutions given in this study for the cases of fluid injection into an interior point and the analytical solutions for either a horizontal or vertical line source with $l/h = 0.1$ and $d/h = 0.1$, respectively. The vertical displacements presented here are non-dimensionalized by $2Gk/Q_0\gamma_w$ where Q_0 is the total volume flow rate for the point source (we omit the negative sign in the displacement results with the understand-

ing that the vertical displacement u_z occurs due to the fluid injection in the negative z -direction). The point source results obtained from the axisymmetric system are consistent with the results obtained from the 3-dimensional model. When the total volume flow rates, $Q_{l/h=0.1}$ and $Q_{d/h=0.1}$, are the same as Q_0 , the results for the horizontal and vertical line source cases $l/h = 0.1$ and $d/h = 0.1$, respectively, also show good agreement with the point source solutions. $Q_{l/h=0.1} = Q_{d/h=0.1} = Q_0$ is valid throughout this study.

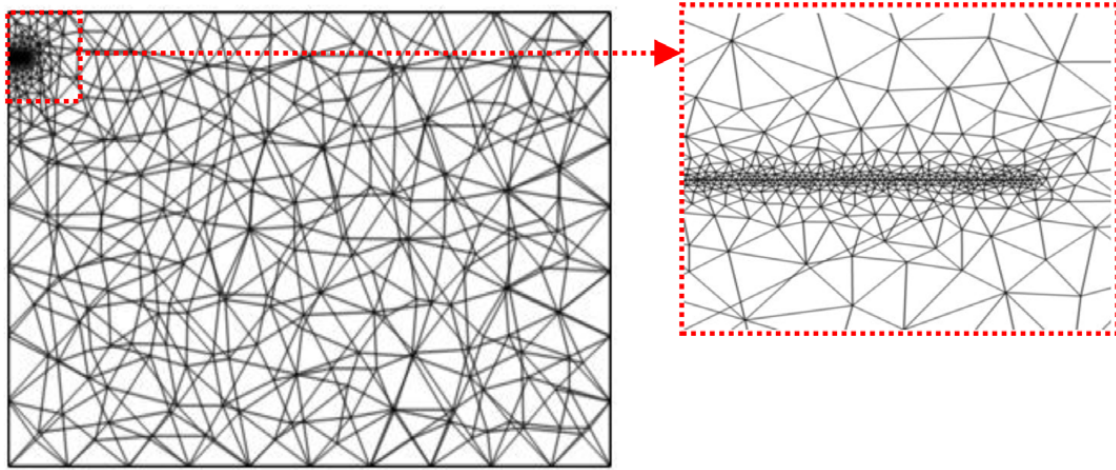


Fig. 4. Mesh configuration of the cross-section (x - z -plane) for the 3-D finite element modelling of the injection problem (11, 616 tetrahedral elements for $l/h = 0.1$).

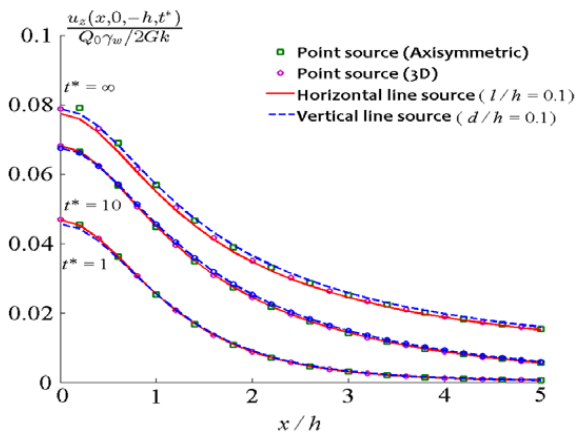


Fig. 5. Comparison of the point source solutions and line source solutions.

5.2. Horizontal line source

5.2.1. Surface displacement

Fig. 6 illustrates the variation in the time-dependent surface displacement $u_z(x, 0, -h, t^*)$ along the x -axis for different values of l/h . Since the horizontal line source solution is obtained by continuously superposing the point source solution, the total volume flow rate Q increases as l/h increases (e.g. $Q_{l/h=5} = 10Q_0$). As expected, Fig. 6 shows that the surface heave increases as l/h increases. Assuming that the surface heave for the case of $l/h = 10$ at $t^* \rightarrow \infty$ is the maximum heave, we observed that, at $t^* = 1$, the surface heave for the case of $l/h = 0.1$ is less than 3% of the maximum heave, while the heave when $l/h = 10$ is approximately 30% of the maximum. At the end of the poromechanical process ($t^* \rightarrow \infty$), the surface heave for the case $l/h = 0.1$ only attains 4% of the maximum heave for the case $l/h = 10$. This implies that the time required to reach a certain degree of surface heave increases as l/h increases. As l/h increases, the surface heave is flattened at the centre and becomes wider in the x -direction. The corresponding computational results are presented as circles and show good agreement (Fig. 6).

The vertical displacements plotted as 3D surfaces are shown in Fig. 7 for different l/h . It is clearly observable

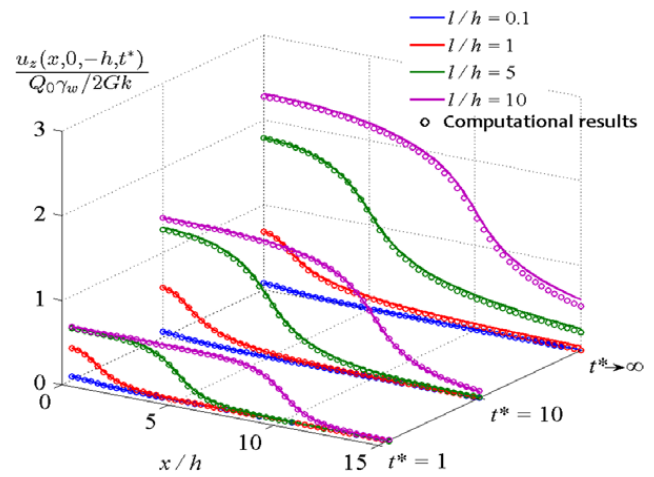


Fig. 6. Time-dependent surface displacements in the x -direction.

that the magnitude of the surface heave increases and the shape becomes wider in the x -direction as l/h increases. However, unlike the results observed in the x -direction, the heave shape does not change with l/h in the y -direction; there is no observable flattening of the centre or widening of the heave in the y -direction.

Fig. 8 shows the non-dimensionalized surface displacement for different Poisson's ratios where the relative line length is $l/h = 0.1$. The surface heave for $(\nu, \nu_u) = (0, 0.01), (0, 0.2),$ and $(0, 0.4)$ are larger than those for $(\nu, \nu_u) = (0.49, 0.5), (0.4, 0.5), (0.2, 0.5)$ and $(0, 0.5)$. The surface heave decreases as ν increases when $\nu_u = 0.5$ and the difference increases to 0.15. The non-dimensionalized surface heave for $(\nu, \nu_u) = (0, 0.5)$ is approximately 0.16 while that for $(\nu, \nu_u) = (0.49, 0.5)$ is less than 0.01. When $\nu = 0$, the surface heave shows a slight decrease as ν_u increases; however, the maximum non-dimensionalized surface heave is the same as that found at 0.16 for $(\nu, \nu_u) = (0, 0.01), (0, 0.2),$ and $(0, 0.4)$ in this study.

5.2.2. Change in pore fluid pressure

In Fig. 9, the changes in pore fluid pressure due to fluid injection into the porous medium for different values of l/h are shown. The total volume flow rate Q increases

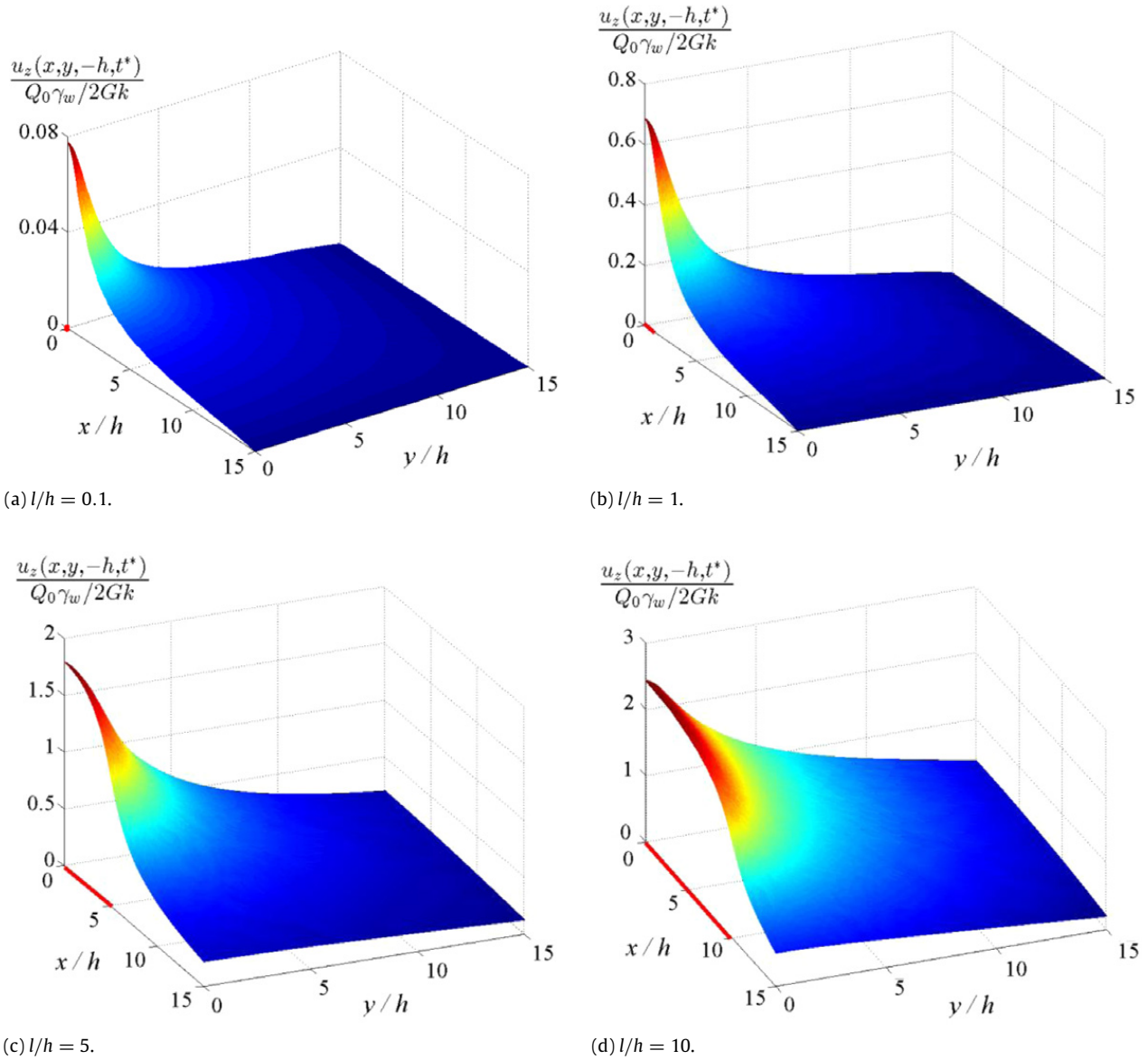


Fig. 7. Surface heave in the positive x - y -plane for different horizontal injection lengths at $t^* \rightarrow \infty$ (red line indicates the injection region). (For interpretation of the references to colour in this figure legend, the reader is referred to the web version of this article.)

with l/h , and therefore the pore fluid pressure also increases as l/h increases. The results for the horizontal line source are compared with the results obtained for the point source problem. We noted that the vertical displacement converges to the point source solution when $l/h = 0.1$; however, the pressure results obtained for the horizontal line source for $l/h = 0.1$ are bounded whereas those obtained for the point source are singular. The corresponding computational results are plotted as dashed lines and they show good agreement with the analytical solutions. The discrepancy between the analytical and computational results is less than 6% excluding the interface.

5.2.3. Change in effective stresses

The change in the effective stress is calculated from the result

$$(\sigma'_{ij})^Q = (\sigma_{ij})^Q - \alpha(p)^Q \delta_{ij} \quad (32)$$

where $(\sigma_{ij})^Q$ and p^Q are the changes in the total stress and pore fluid pressure due to fluid injection and α is the Biot parameter. The injection of fluids into the porous medium increases the pore fluid pressure surrounding the injection region, and, therefore, the effective stress is expected to decrease in the injection zone. The results obtained at $x = y = 0$ are shown in Figs. 10 and 11 for $(\sigma'_{xx})^Q$ and $(\sigma'_{zz})^Q$, respectively. Both results give negative values, which indicates that there is a decrease in the effective stress of the porous medium. The computational solutions are also plotted in dashed lines on the figures and the agreement with the analytical solutions is generally good for results obtained in both the x and z -directions.

5.3. Vertical line source

Fig. 12 presents the non-dimensionalized surface displacements for the vertical line source problem for different values of non-dimensional time t^* . The illustrated

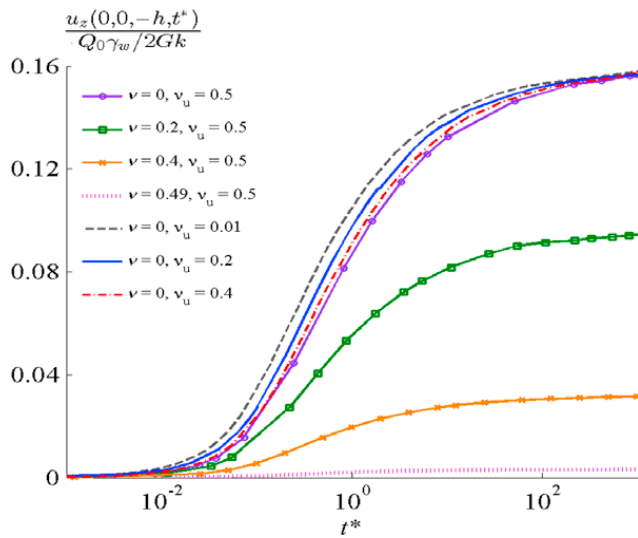


Fig. 8. Surface settlement for different Poisson's ratios when $l/h = 0.1$.

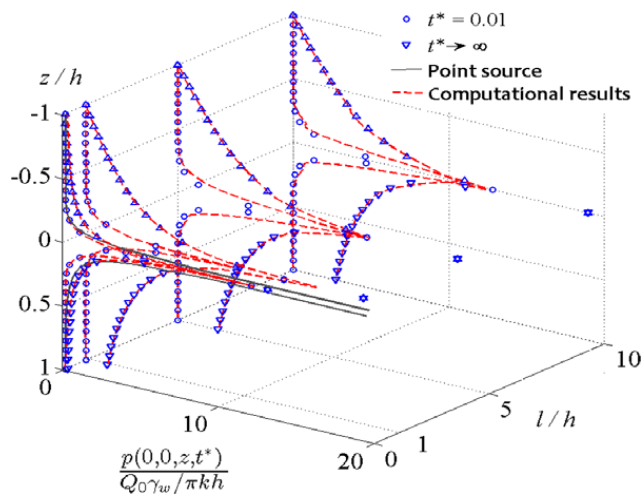


Fig. 9. Changes in pore fluid pressure.

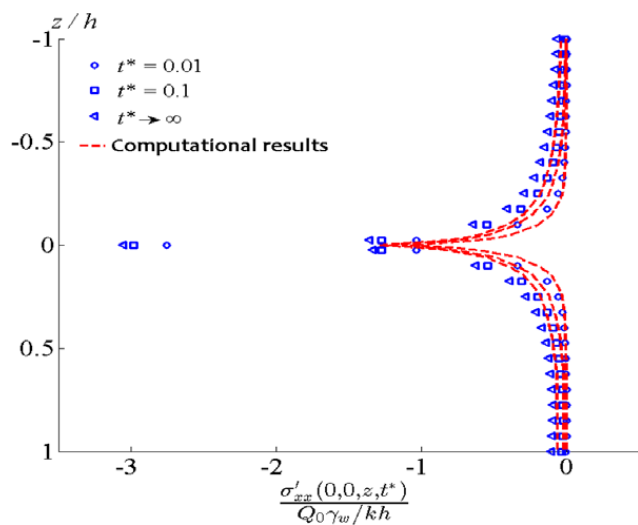


Fig. 10. Changes in effective stress in the x-direction.

results were obtained by varying the length of the vertical line injection region, d . Although this problem is consid-

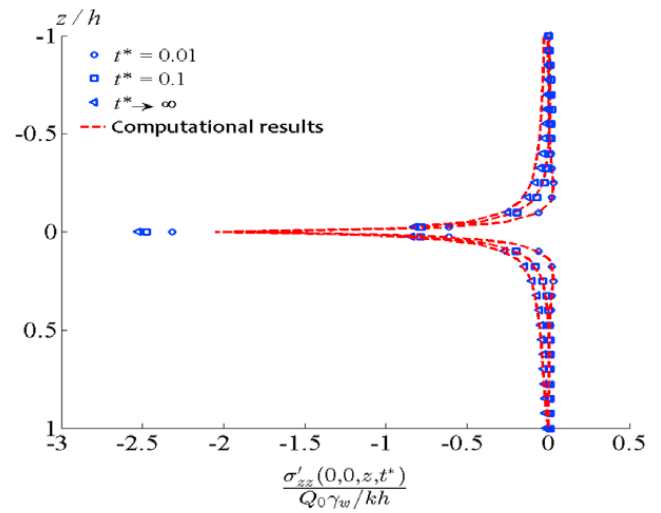


Fig. 11. Changes in effective stress in the z-direction.

ered to be 3-dimensional in this study, it is an axisymmetric problem, and the results obtained in the x - and y -directions are the same. It can be seen from Fig. 12 that the magnitude of the surface heave increases as d/h increases. In the case of the horizontal line source, the surface heave flattened at the centre and became wider as l/h increased. However, in the case of the vertical source problem, no widening of the heave was observed and the flattening at the centre is comparatively smaller than for the horizontal line source problem. Also, comparing the results for the cases $d/h = 1, 5$ and 10 with those for the horizontal line source problem, it is observed that the magnitudes of the surface heave associated with the vertical line source injection were larger than those for the horizontal line source problem. The corresponding computational results are plotted as circles in Fig. 12. The agreement between the analytical results and the computational results is good.

6. The stress state during injection

The injection of fluids into the interior of a fluid-saturated poroelastic medium can alter the stress state in the halfspace region. In such studies, it is implicitly assumed that the porous medium is hydraulically and mechanically homogeneous and that the injection does not result in changes to the hydro-mechanical properties of the geomaterial. Experimental and theoretical investigations suggest that material heterogeneity can be important to poromechanical aspects of the problem^{48,49} and that alteration in the stress state can result in alteration to the mechanical and fluid transmissivity properties.^{50–57} The poroelastic analysis of the injection process can be used to examine the potential for development of failure in the fluid-saturated medium at a specific location. The development of failure will be governed by the effective stress state in the fluid-saturated medium, which consists of the in situ effective geostatic stress state, $(\sigma'_{ij})^0(x, y, z, t)$ and the effective stress induced by the fluid injection process, $[\sigma'_{ij}(x, y, z, t)]^Q$. The in situ effective stress state is assumed to be geostatic and given by

$$(\sigma'_{ij})^0(x, y, z, t)$$

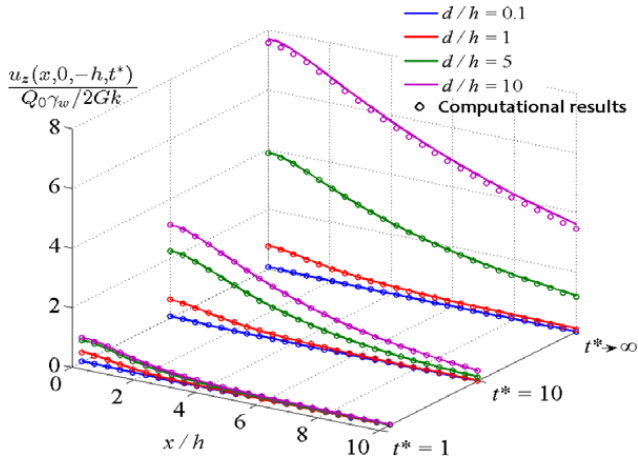


Fig. 12. Normalized surface displacements in the x-direction.

$$= \begin{bmatrix} (\gamma_s - \gamma_w)z & 0 & 0 \\ 0 & \left(\frac{\nu}{1-\nu}\right)(\gamma_s - \gamma_w)z & 0 \\ 0 & 0 & \left(\frac{\nu}{1-\nu}\right)(\gamma_s - \gamma_w)z \end{bmatrix} \quad (33)$$

where γ_s is the saturated unit weight of the poroelastic medium. The effective stress state after injection is given by

$$\sigma'_{ij} = (\sigma'_{ij})^0 + (\sigma'_{ij})^Q. \quad (34)$$

The susceptibility to fracture initiation during injection can be determined by prescribing a failure criterion and applying the criterion to a critical location in the vicinity of the injection zone. The failure criterion chosen for the analysis of fracture is the Hoek–Brown⁵⁸ criterion, which is used quite extensively in rock mechanics:

$$\sigma'_1 = \sigma'_3 + \sigma'_{UCS} \left(m_i \frac{\sigma'_3}{\sigma'_{UCS}} + 1 \right)^{0.5} \quad (35)$$

where σ'_{UCS} is the uniaxial compressive strength of the intact rock material and m_i is the Hoek–Brown parameter. In this study, we have used $\sigma'_{UCS} = 48.9 \text{ MPa}$ ⁵⁹ and $m_i = 7.8e^{-\sigma_3/22.5}$ ⁶⁰ to obtain the Hoek–Brown failure criterion for Indiana limestone. Using a linear approximation, we modify the Hoek–Brown criterion as a form of the K_f –line which is a function of $p' = (\sigma'_1 + \sigma'_3)/2$ and $q' = (\sigma'_1 - \sigma'_3)/2$ (Fig. 13).

We assume that the injection site is in the layer of Indiana Limestone that has the elastic properties given in Section 5 and a saturated unit weight of 26500 N/m^3 . When fluid is injected into a horizontal line of length 200 m (2l) at a depth of 1000m, the maximum and minimum initial effective stresses are 16.69 MPa and 5.56 MPa at the injection site. Assuming that $\sigma'_1 = \sigma'_{zz}$, $\sigma'_2 = \sigma'_{yy}$ and $\sigma'_3 = \sigma'_{xx}$, the stress path is a line with a slope of

$$\frac{dq'}{dp'} = \frac{d\sigma'_{zz} - d\sigma'_{xx}}{d\sigma'_{zz} + d\sigma'_{xx}}. \quad (36)$$

For the point at the centre of the injection region, the failure analysis is shown in Fig. 13 for different volume flow rates, Q . It is observed that the slope of the stress path does not change; however, the stress path approaches the

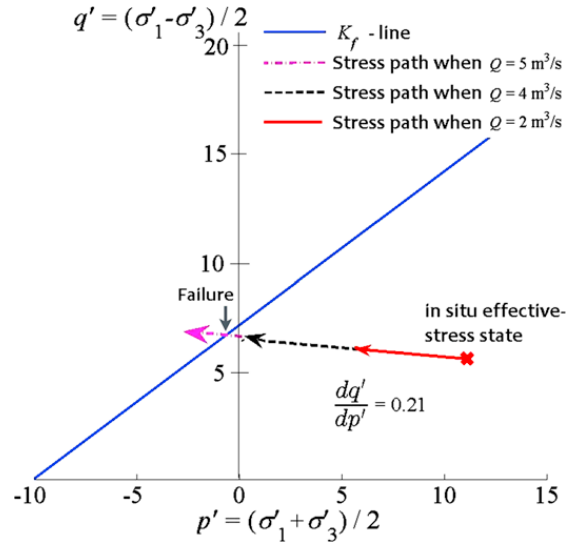


Fig. 13. Modified Hoek–Brown failure criterion and stress paths.

failure criterion indicated by proximity to the K_f –line as the volume flow rate, Q , increases. In this study, the failure at the centre of the injection location can occur when Q exceeds $5 \text{ m}^3/\text{s}$.

7. Conclusions

In this paper, the analytical solutions for the poroelastic problem of fluid injection along horizontal or vertical line elements were developed by using the analytical results for the point source solutions. Assuming that the lines consist of a number of points, we superpose the point source solutions to formulate the solutions for the horizontal and vertical line sources. The influence of the length of the injection line is investigated on the surface displacement, pore fluid pressure and effective stress. For a total Q , larger surface heave is observed as the length of the injection line increases horizontally or vertically. The pore fluid pressure surrounding the injection region increases due to the fluid injection. Also, we observed that there is a larger change in the pore fluid pressure as the injection line length increases. The increase in pore fluid pressure results in a decrease in the effective stress. The possibility of injection-induced failure is also examined by applying the Hoek–Brown failure criterion.

The superposition technique introduced in this study can be conveniently applied to other distributed injection problems including circular, disc-shaped and non-axis-aligned lines. Also, the solutions presented here can be used to accommodate fluid withdrawal problems. Since the analysis is restricted to poroelastic behaviour of the fluid-saturated geomaterial, when the injection ceases the ground heave will gradually reduce to zero and the rate at which the ground heave recovers can be examined using the present formulation. The analytical solutions will serve as a useful first approximation for analogous but more complex geologic sequestration problems.

$$\begin{aligned}
 \frac{u_z^H(x, y, z, t)}{Q_0 \gamma_w \alpha / 2G(2\pi)^2 k} &= \int_{\zeta-i\infty}^{\zeta+i\infty} \int_{-\infty}^{\infty} \int_{-\infty}^{\infty} e^{i(ux+vy)} \\
 &\times \left\{ \left(\frac{e^{-\sqrt{u^2+v^2}h} - e^{-\varphi h}}{\eta \Gamma(\varphi - \sqrt{u^2+v^2})^2 - \eta(\varphi^2 - \sqrt{u^2+v^2}^2) + \sqrt{u^2+v^2}(\varphi - \sqrt{u^2+v^2})} \right) \right. \\
 &\times \left[(\sqrt{u^2+v^2}(z+h)(\Gamma-1) - \Gamma)e^{-\sqrt{u^2+v^2}(z+h)} + \frac{(2\eta\sqrt{u^2+v^2}\Gamma - \sqrt{u^2+v^2})}{\eta(\varphi^2 - \sqrt{u^2+v^2}^2)} \right. \\
 &\times \left. \left. (\varphi e^{-\varphi(z+h)} - \sqrt{u^2+v^2}e^{-\sqrt{u^2+v^2}(z+h)}) \right] + \sqrt{u^2+v^2}(e^{-\sqrt{u^2+v^2}(z+h)} - e^{-\sqrt{u^2+v^2}(z-h)}) \right. \\
 &\times \left. \frac{e^{-\sqrt{u^2+v^2}h}}{2\eta\sqrt{u^2+v^2}(\varphi^2 - \sqrt{u^2+v^2}^2)} + \varphi(e^{-\varphi(z+h)} - e^{-\varphi(z-h)}) \frac{-e^{-\varphi h}}{2\eta\varphi(\varphi^2 - \sqrt{u^2+v^2}^2)} \right\} \\
 &\times \frac{e^{st}}{s} dudvds \tag{A.1}
 \end{aligned}$$

Box IV.

$$\begin{aligned}
 \frac{p^L(x, y, z, t)}{Q_0 \gamma_w / (2\pi)^2 k} &= \int_{\zeta-i\infty}^{\zeta+i\infty} \int_{-\infty}^{\infty} \int_{-\infty}^{\infty} e^{i(ux+vy)} \left\{ \left(\frac{e^{-\varphi z - 2\varphi h} - e^{\varphi z}}{2\varphi} \right) \right. \\
 &+ \left. \left[\frac{(2\eta\Gamma\sqrt{u^2+v^2} - \sqrt{u^2+v^2})(e^{-\sqrt{u^2+v^2}h} - e^{-\varphi h})(e^{-\sqrt{u^2+v^2}(z+h)} - e^{-\varphi(z+h)})}{\eta\Gamma(\varphi - \sqrt{u^2+v^2})^2 - \eta(\varphi^2 - \sqrt{u^2+v^2}^2) + \sqrt{u^2+v^2}(\varphi - \sqrt{u^2+v^2})} \right] \right\} \frac{e^{st}}{s} dudvds \tag{A.2}
 \end{aligned}$$

Box V.

$$\begin{aligned}
 \frac{p^H(x, y, z, t)}{Q_0 \gamma_w / (2\pi)^2 k} &= \int_{\zeta-i\infty}^{\zeta+i\infty} \int_{-\infty}^{\infty} \int_{-\infty}^{\infty} e^{i(ux+vy)} \left\{ \left(\frac{e^{-\varphi z - 2\varphi h} - e^{-\varphi z}}{2\varphi} \right) \right. \\
 &+ \left. \left[\frac{(2\eta\Gamma\sqrt{u^2+v^2} - \sqrt{u^2+v^2})(e^{-\sqrt{u^2+v^2}h} - e^{-\varphi h})(e^{-\sqrt{u^2+v^2}(z+h)} - e^{-\varphi(z+h)})}{\eta\Gamma(\varphi - \sqrt{u^2+v^2})^2 - \eta(\varphi^2 - \sqrt{u^2+v^2}^2) + \sqrt{u^2+v^2}(\varphi - \sqrt{u^2+v^2})} \right] \right\} \frac{e^{st}}{s} dudvds \tag{A.3}
 \end{aligned}$$

Box VI.

$$\begin{aligned}
 \frac{\sigma_{xx}^L(x, y, z, t)}{Q_0 \gamma_w \alpha / (2\pi)^2 k} &= \int_{\zeta-i\infty}^{\zeta+i\infty} \int_{-\infty}^{\infty} \int_{-\infty}^{\infty} e^{i(ux+vy)} \left\{ \left[\sqrt{u^2+v^2}(2\Gamma - (z+h)\sqrt{u^2+v^2}(\Gamma-1) - 2) \right. \right. \\
 &\times \left(\frac{e^{-\sqrt{u^2+v^2}h} - e^{-\varphi h}}{\eta\Gamma(\varphi - \sqrt{u^2+v^2})^2 - \eta(\varphi^2 - \sqrt{u^2+v^2}^2) + \sqrt{u^2+v^2}(\varphi - \sqrt{u^2+v^2})} \right) e^{-\sqrt{u^2+v^2}(z+h)} \\
 &+ \frac{\sqrt{u^2+v^2}(2\eta\Gamma-1)}{\eta(\varphi^2 - \sqrt{u^2+v^2}^2)} (\sqrt{u^2+v^2}e^{-\sqrt{u^2+v^2}(z+h)} - \varphi^2 e^{-\varphi(z+h)}) \\
 &\times \left(\frac{e^{-\sqrt{u^2+v^2}h} - e^{-\varphi h}}{\eta\Gamma(\varphi - \sqrt{u^2+v^2})^2 - \eta(\varphi^2 - \sqrt{u^2+v^2}^2) + \sqrt{u^2+v^2}(\varphi - \sqrt{u^2+v^2})} \right) \\
 &+ \left. \left. \frac{\varphi^2(e^{-\varphi(z+2h)} - e^{\varphi z})}{2\eta\varphi(\varphi^2 - \sqrt{u^2+v^2}^2)} - \frac{\sqrt{u^2+v^2}(e^{-\sqrt{u^2+v^2}(z+2h)} - e^{\sqrt{u^2+v^2}z})}{2\eta\sqrt{u^2+v^2}(\varphi^2 - \sqrt{u^2+v^2}^2)} \right] \right\} \frac{e^{st}}{s} dudvds \tag{A.4}
 \end{aligned}$$

Box VII.

$$\begin{aligned} \frac{\sigma_{xx}^H(x, y, z, t)}{Q_0 \gamma_w \alpha / (2\pi)^2 k} &= \int_{\zeta-i\infty}^{\zeta+i\infty} \int_{-\infty}^{\infty} \int_{-\infty}^{\infty} e^{i(ux+vy)} \left\{ \left[\sqrt{u^2 + v^2} (2\Gamma - (z+h)\sqrt{u^2 + v^2}(\Gamma - 1) - 2) \right. \right. \\ &\times \left(\frac{e^{-\sqrt{u^2+v^2}h} - e^{-\varphi h}}{\eta\Gamma(\varphi - \sqrt{u^2 + v^2})^2 - \eta(\varphi^2 - \sqrt{u^2 + v^2}^2) + \sqrt{u^2 + v^2}(\varphi - \sqrt{u^2 + v^2})} \right) e^{-\sqrt{u^2+v^2}(z+h)} \\ &+ \frac{\sqrt{u^2 + v^2}(2\eta\Gamma - 1)}{\eta(\varphi^2 - \sqrt{u^2 + v^2}^2)} (\sqrt{u^2 + v^2}^2 e^{-\sqrt{u^2+v^2}(z+h)} - \varphi^2 e^{-\varphi(z+h)}) \\ &\times \left(\frac{e^{-\sqrt{u^2+v^2}h} - e^{-\varphi h}}{\eta\Gamma(\varphi - \sqrt{u^2 + v^2})^2 - \eta(\varphi^2 - \sqrt{u^2 + v^2}^2) + \sqrt{u^2 + v^2}(\varphi - \sqrt{u^2 + v^2})} \right) \\ &\left. \left. + \frac{\varphi^2(e^{-\varphi(z+2h)} - e^{-\varphi z})}{2\eta\varphi(\varphi^2 - \sqrt{u^2 + v^2}^2)} - \frac{\sqrt{u^2 + v^2}(e^{-\sqrt{u^2+v^2}(z+2h)} - e^{-\sqrt{u^2+v^2}z})}{2\eta\sqrt{u^2 + v^2}(\varphi^2 - \sqrt{u^2 + v^2}^2)} \right] \right\} \frac{e^{st}}{s} dudvds \quad (A.5) \end{aligned}$$

Box VIII.

$$\begin{aligned} \frac{\sigma_{zz}^L(x, y, z, t)}{Q_0 \gamma_w \alpha / (2\pi)^2 k} &= \int_{\zeta-i\infty}^{\zeta+i\infty} \int_{-\infty}^{\infty} \int_{-\infty}^{\infty} e^{i(ux+vy)} \left\{ \left[\sqrt{u^2 + v^2}^2 \left((z+h)(\Gamma - 1) - \frac{\sqrt{u^2 + v^2}(2\eta\Gamma - 1)}{\eta(\varphi^2 - \sqrt{u^2 + v^2}^2)} \right) \right. \right. \\ &\times \left(\frac{e^{-\sqrt{u^2+v^2}h} - e^{-\varphi h}}{\eta\Gamma(\varphi - \sqrt{u^2 + v^2})^2 - \eta(\varphi^2 - \sqrt{u^2 + v^2}^2) + \sqrt{u^2 + v^2}(\varphi - \sqrt{u^2 + v^2})} \right) e^{-\sqrt{u^2+v^2}(z+h)} \\ &+ \frac{\sqrt{u^2 + v^2}^3(2\eta\Gamma - 1)}{\eta(\varphi^2 - \sqrt{u^2 + v^2}^2)} \left(\frac{e^{-\sqrt{u^2+v^2}h} - e^{-\varphi h}}{\eta\Gamma(\varphi - \sqrt{u^2 + v^2})^2 - \eta(\varphi^2 - \sqrt{u^2 + v^2}^2) + \sqrt{u^2 + v^2}(\varphi - \sqrt{u^2 + v^2})} \right) e^{-\varphi(z+h)} \\ &\left. \left. + \frac{\sqrt{u^2 + v^2}}{2\eta(\varphi^2 - \sqrt{u^2 + v^2}^2)} (e^{-\sqrt{u^2+v^2}(z+2h)} - e^{-\sqrt{u^2+v^2}z}) + \frac{\sqrt{u^2 + v^2}^2}{2\eta\varphi(\varphi^2 - \sqrt{u^2 + v^2}^2)} (e^{\varphi z} - e^{-\varphi(z+2h)}) \right] \right\} \frac{e^{st}}{s} dudvds \quad (A.6) \end{aligned}$$

Box IX.

$$\begin{aligned} \frac{\sigma_{zz}^H(x, y, z, t)}{Q_0 \gamma_w \alpha / (2\pi)^2 k} &= \int_{\zeta-i\infty}^{\zeta+i\infty} \int_{-\infty}^{\infty} \int_{-\infty}^{\infty} e^{i(ux+vy)} \left\{ \left[\sqrt{u^2 + v^2}^2 \left((z+h)(\Gamma - 1) - \frac{\sqrt{u^2 + v^2}(2\eta\Gamma - 1)}{\eta(\varphi^2 - \sqrt{u^2 + v^2}^2)} \right) \right. \right. \\ &\times \left(\frac{e^{-\sqrt{u^2+v^2}h} - e^{-\varphi h}}{\eta\Gamma(\varphi - \sqrt{u^2 + v^2})^2 - \eta(\varphi^2 - \sqrt{u^2 + v^2}^2) + \sqrt{u^2 + v^2}(\varphi - \sqrt{u^2 + v^2})} \right) e^{-\sqrt{u^2+v^2}(z+h)} \\ &+ \frac{\sqrt{u^2 + v^2}^3(2\eta\Gamma - 1)}{\eta(\varphi^2 - \sqrt{u^2 + v^2}^2)} \left(\frac{e^{-\sqrt{u^2+v^2}h} - e^{-\varphi h}}{\eta\Gamma(\varphi - \sqrt{u^2 + v^2})^2 - \eta(\varphi^2 - \sqrt{u^2 + v^2}^2) + \sqrt{u^2 + v^2}(\varphi - \sqrt{u^2 + v^2})} \right) e^{-\varphi(z+h)} \\ &\left. \left. + \frac{\sqrt{u^2 + v^2}}{2\eta(\varphi^2 - \sqrt{u^2 + v^2}^2)} (e^{-\sqrt{u^2+v^2}(z+2h)} - e^{-\sqrt{u^2+v^2}z}) + \frac{\sqrt{u^2 + v^2}^2}{2\eta\varphi(\varphi^2 - \sqrt{u^2 + v^2}^2)} (e^{-\varphi z} - e^{-\varphi(z+2h)}) \right] \right\} \frac{e^{st}}{s} dudvds \quad (A.7) \end{aligned}$$

Box X.

Acknowledgements

The work described in this paper was initiated through a NSERC Discovery Grant awarded to A.P.S. Selvadurai. The first author is grateful to the McGill Engineering Doctoral Award and GEC3 Graduate Student Stipend.

Disclaimer

The use of the computational code COMSOL™ is for demonstrational purpose only. The authors neither advocate nor recommend the use of the code without conducting suitable validation procedures to test the accuracy of the code in a rigorous fashion.

Appendix

The displacements in the z-direction, the change in pore fluid pressure, and the effective stresses in three-dimensional forms are given by equations in Boxes IV, V, VI, VII, VIII, IX and X).

References

- [1] Rutqvist J. The geomechanics of CO₂ storage in deep sedimentary formations. *Geotech. Geol. Eng.* 2012;30:515–551.
- [2] Selvadurai APS. Heave of a surficial rock layer due to pressures generated by injected fluids. *Geophys. Res. Lett.* 2009;36(14):L14302.
- [3] Selvadurai APS. A geophysical application of an elastostatic contact problem. *Math. Mech. Solids* 2013;18(2):192–203.
- [4] Selvadurai APS, Nguyen TS. Computational modelling of isothermal consolidation of fractured porous media. *Comput. Geotech.* 1995;17:39–73.
- [5] Selvadurai APS, Nguyen TS. Scoping analyses of the coupled thermal-hydrological-mechanical behavior of the rock mass around a nuclear fuel waste repository. *Eng. Geol.* 1996;47(4):379–400.
- [6] Rutqvist J, Börgesson L, Kobayashi A, Jing L, Nguyen TS, Noorshad J, Tsang C-F. Thermohydromechanics of partially saturated geological media: governing equations and formulation of four finite element models. *Int. J. Rock Mech. Min. Sci.* 2001;38:105–127.
- [7] Selvadurai APS. The advective transport of a chemical from a cavity in a porous medium. *Comput. Geotechnics* 2002;29:525–546.
- [8] Selvadurai APS. Contaminant migration from an axisymmetric source in a porous medium. *Water Resour. Res.* 2003;39(8):1204.
- [9] Selvadurai APS. Gravity-driven advective transport during deep geological disposal of contaminants. *Geophys. Res. Lett.* 2006;33:L08408.
- [10] Tsang C-F, Birkholzer J, Rutqvist J. A comparative review of hydrologic issues involved in geologic storage of CO₂ and injection disposal of liquid waste. *Enviro. Geol.* 2008;54(8):1723–1737.
- [11] Selvadurai APS, Suvorov AP. Boundary heating of poro-elastic and poro-elasto-plastic spheres, Proceedings of the Royal Society A: Mathematical. *Phys. Eng. Sci.* 2012;468(2145):2779–2806.
- [12] Selvadurai APS, Suvorov AP. Thermo-poromechanics of a fluid-filled cavity in a fluid-saturated geomaterial. *Proc. R. Soc. Lond. Ser. A: Math. Phys. Eng. Sci.* 2014;470(2163):20130634.
- [13] Vasco DW, Rucci A, Ferretti A, Novali F, Bissel RC, Ringrose PS, Mathieson AS, Wright IW. Satellite-based measurements of surface deformation reveal fluid flow associated with the geological storage of carbon dioxide. *Geophys. Res. Lett.* 2010;37:L03303.
- [14] Geertsma J. Land subsidence above compacting oil and gas reservoirs. *J. Pet. Technol.* 1973;25:734–744.
- [15] Segall P. Induced stresses due to fluid extraction from axisymmetric reservoirs. *Pure Appl. Phys.* 1992;139:535–560.
- [16] Segall P, Fitzgerald SD. A note on induced stress changes in hydrocarbon and geothermal reservoirs. *Tectonophysics* 1998;289(1–3):117–128.
- [17] Biot MA. General theory of three-dimensional consolidation. *J. Appl. Phys.* 1941;12:155–164.
- [18] Rice JR, Cleary MP. Some basic stress diffusion solutions for fluid-saturated elastic porous media with compressible constituents. *Rev. Geophys.* 1976;14(2):227–241.
- [19] Detournay E, Cheng A. *Comprehensive rock engineering: Principles, practice and projects*. In: Hudson JA, ed. Fundamentals of Poroelasticity, vol. 1. Oxford: Pergamon Press; 1993:113–171.
- [20] Coussy O. *Mechanics of Porous Media*. New York: Wiley; 1995.
- [21] Selvadurai APS, ed. *Mechanics of Poroelastic Media*. Dordrecht: The Netherlands: Kluwer Academic; 1996.
- [22] Selvadurai APS. The analytical method in geomechanics. *Appl. Mech. Rev.* 2007;60(3):87–106.
- [23] Selvadurai APS, Yue ZQ. On the indentation of a poroelastic layer. *Int. J. Numer. Anal. Methods Geomech.* 1994;18:161–175.
- [24] Yue ZQ, Selvadurai APS, Law KT. Excess pore pressure in a poroelastic seabed saturated with a compressible fluid. *Can. Geotech. J.* 1994;31(6):989–1003.
- [25] Selvadurai APS, Shirazi A. Mandel-Cryer effects in fluid inclusions in damage-susceptible poroelastic geologic media. *Comput. Geotech.* 2004;31:285–300.
- [26] Verruijt A. *Theory and Problems of Poroelasticity*. Delft, The Netherlands: Delft University of Technology; 2013.
- [27] Bear J. *Dynamics of Fluids in Porous Media*. New York: Dover Publications; 1972.
- [28] Booker JR, Carter JP. Analysis of a point sink embedded in a porous elastic half space. *Int. J. Numer. Anal. Methods Geomech.* 1986;10:137–150.
- [29] Booker JR, Carter JP. Elastic consolidation around a point sink embedded in a half-space with anisotropic permeability. *Int. J. Numer. Anal. Methods Geomech.* 1987;11(1):61–77.
- [30] Kanok-Nukulchai W, Chau KT. Point sink fundamental solutions for subsidence prediction. *J. Eng. Mech.* 1990;116(5):1176–1182.
- [31] Rutqvist J, Vasco DW, Meyer L. Coupled reservoir geomechanical analysis of the potential for tensile and shear failure associated with CO₂ injection at In Salah, Algeria. *Energy Procedia* 2008;1:1847–1854.
- [32] Rutqvist J, Birkholzer JT, Tsang C-F. Coupled reservoir-geomechanical analysis of the potential for tensile and shear failure associated with CO₂ injection in multilayered reservoir-caprock systems. *Int. J. Rock Mech. Min. Sci.* 2008;45(2):132–143.
- [33] Segall P, Grasso JR, Mossop A. Poroelastic stressing and induced seismicity near the Lacq gas field, southwestern France. *J. Geophys. Res.* 1994;99:15423–15438.
- [34] Rice JR. Heating and weakening of faults during earthquake slip. *J. Geophys. Res.* 2006;111:B05311.
- [35] Yue ZQ, Selvadurai APS. Axisymmetric indentation of a multilayered poroelastic solid. *Mechanics of Poroelastic Media*. In: Selvadurai APS, ed. Dordrecht, The Netherlands: Kluwer Academic; 1996.
- [36] Skempton AW. The pore-pressure coefficients A and B. *Geotechnique* 1954;4:143–147.
- [37] Wang HF. *Theory of Linear Poroelasticity: with Applications to Geomechanics and Hydrogeology*. Princeton: Princeton University Press; 2000.
- [38] McNamee J, Gibson RE. Displacement functions and linear transforms applied to diffusion through porous elastic media. *Q. J. Mech. Appl. Math.* 1960;13:98–111.
- [39] McNamee J, Gibson RE. Plane strain and axially symmetric problems of consolidation of a semi-infinite clay stratum. *Q. J. Mech. Appl. Math.* 1960;13:210–227.
- [40] Chau KT. Fluid point source and point forces in linear elastic diffusive half-space. *Mech. Mater.* 1996;23:241–253.
- [41] Chen GJ. Steady state solutions of multilayered and cross-anisotropic poroelastic half-space due to a point sink. *Int. J. Geomech.* 2005;5:45–57.
- [42] Selvadurai APS, Kim J. Ground subsidence due to uniform fluid extraction over a circular region within an aquifer. *Adv. Water Resour.* 2015;78:50–59.
- [43] Sneddon IN. *Fourier Transformations*. New York, NY: McGraw - Hill; 1951.
- [44] Selvadurai APS. *Partial Differential Equations in Mechanics I: Fundamentals, Laplace's Equation, Diffusion Equation, Wave Equation*. Berlin: Springer-Verlag; 2000.
- [45] Crump K. Numerical inversion of Laplace transforms using a Fourier series approximation. *J. Assoc. Comput. Mach.* 1976;23(1):89–96.
- [46] Hart DJ, Wang HF. Laboratory measurements of a complete set of poroelastic moduli for Berea sandstone and Indiana limestone. *J. Geophys. Res.* 1995;100(B9):17741–17751.
- [47] Selvadurai APS, Najari M. On the interpretation of hydraulic pulse tests on rock specimens. *Adv. Water Resources* 2013;53:139–149.
- [48] Selvadurai APS, Selvadurai PA. Surface permeability tests: experiments and modelling for estimating effective permeability. *Proceedings of the Royal Society A: Mathematical, Phys. Eng. Sci.* 2010;466:2819–2846.
- [49] Selvadurai PA, Selvadurai APS. On the effective permeability of a heterogeneous porous medium: the role of the geometric mean. *Phil. Mag.* 2014;94(20):2318–2338.
- [50] Selvadurai APS. Stationary damage modelling of poroelastic contact. *Int. J. Solids Struct.* 2004;4:2043–2064.
- [51] Selvadurai APS, Carnaffan P. A transient pressure pulse method for the measurement of permeability of a cement grout. *Can. J. Civ. Eng.* 1997;24:489–502.
- [52] Selvadurai APS, Boulon MJ, Nguyen TS. The permeability of an intact granite. *Pure Appl. Geophys.* 2005;162:373–407.
- [53] Selvadurai APS. Fluid leakage through fractures in an impervious caprock embedded between two geologic aquifers. *Adv. Water Resour.* 2012;41:76–83.
- [54] Selvadurai APS, Letendre A, Hekimi B. Axial flow hydraulic pulse testing of an argillaceous limestone. *Environ. Earth Sci.* 2011;64:2047–2058.
- [55] Selvadurai APS. Normal stress-induced permeability hysteresis of a fracture in a granite cylinder. *Geofluids, Special Issue on Crustal Permeability* 2015;15:37–47.
- [56] Massart TJ, Selvadurai APS. Computational homogenization based evaluation of damage-induced permeability evolution in quasi-brittle geomaterials. *J. Geophys. Res.* 2012;B117:B07207.

- [57] Massart TJ, Selvadurai APS. Computational modelling of crack-induced permeability evolution in granite with dilatant cracks. *Int. J. Rock Mechanics and Mining Sciences* 2014;70:593–604.
- [58] Hoek E, Carranza-Torres C, Corkum B. Hoek–Brown criterion. *Proc. NARMS-Tac* 2002;267–273.
- [59] Hoek E. Strength of jointed rock masses. *Geotechnique* 1983;33(3): 187–223.
- [60] Peng J, Rong G, Cai M, Wang XJ, Zhou CB. An empirical failure criterion for intact rocks. *Rock Mechanics and Rock Engineering* 2014; 47:347–356.